# Adaptive Kernel Operator Learning for Spatiotemporal Full-Field Reliability Analysis with Mixed Random Inputs

Zhao Liu, Kaiwen Li, Ping Zhu
*State Key Laboratory of Mechanical System and Vibration*
*National Engineering Research Center of Automotive Power and Intelligent Control*
*Shanghai Jiao Tong University, Shanghai 200240, PR China*

**Abstract.** The material properties and external loads of engineering structures inevitably exhibit significant spatial and temporal variability; simplifying these into homogeneous random variables severely underestimates failure probability by neglecting localized weak regions. Conventional surrogate approaches address this by incorporating spatial random fields, yet first discretize them via spectrum methods, introducing truncation errors that become prohibitive for fields with short correlation lengths. This paper proposes a kernel operator learning framework for spatiotemporal full-field reliability analysis that encodes all three categories of uncertain inputs, namely, random variables, stochastic processes, and spatial random fields, through anisotropic product kernels on a latent Gaussian process regressor, bypassing explicit dimensionality reduction. An active learning strategy is further developed, combining an integrated variance reduction term weighted toward the zero level set with a sign-misclassification exploitation term, terminated by a level-set stability criterion. The framework is validated on benchmark problems with mixed random inputs, demonstrating accurate full-field failure probability estimation with a small number of training samples.

**Keywords:** Spatiotemporal full-field reliability analysis, Operator learning, Kernel methods, Gaussian process, Active learning

## 1. Introduction

In critical fields such as aerospace and civil engineering, the material properties of engineering structures (e.g., elastic modulus, strength) and external loads (e.g., wind loads, corrosive environments) inevitably exhibit significant temporal and spatial variability. Catastrophic failure under such conditions carries severe safety and economic consequences. Ensuring structural integrity therefore requires a reliability framework that can represent both the spatial variability and time evolution of material properties and loads, while remaining computationally tractable for large-scale finite element models.

Traditional time-variant reliability analysis methods, including **first-passage-based approaches** (Li et al., 2022) and **extreme value-based approaches** (Cao et al., 2022), primarily account for stochastic processes while treating structural properties as spatially homogeneous, which is known to severely underestimate failure probability by ignoring localized weak regions (Dimitrov et al., 2017; Lu et al., 2023). Spatiotemporal full-field reliability analysis extends this setting by additionally incorporating spatial random fields, tracking failure regions that migrate across the structure, the so-called "moving hotspots" phenomenon (Hu et al., 2026). Analytical extensions of the first-passage approach to this setting (Lu et al., 2023) rely on strong independence assumptions and are limited to small failure probabilities, while extreme value-based approaches become computationally intractable for large-scale finite element models, motivating surrogate-based methods.

To address this challenge, active-learning Kriging models (Zhan and Xiao, 2025; Zhan et al., 2026) and physics-informed neural networks (PINNs) (Zhang and Shafieezadeh, 2022; Roy et al., 2024) have been introduced as surrogates. However, the system responses constructed by these methods typically lack spatial information and fail to identify the critical failure domains. Full-field surrogate models, by contrast, map random inputs to the complete spatiotemporal response field, providing robust support for failure location prediction and critical domain prognosis (Zhao et al., 2025; Li and Ding, 2026). Notably, Li and Ding proposed AER-GP, which uses a dual-order-reduced Gaussian process via PCA to efficiently predict full-field responses, achieving accurate critical domain prognosis with very few training samples.

A key challenge in constructing full-field surrogates for spatiotemporal reliability analysis lies in that the simultaneous presence of three categories of random inputs: finite-dimensional random variables $X(\omega)$, stochastic processes $Y(t;\omega)$, and spatial random fields $Z(\mathbf{z};\omega)$. Classical surrogate approaches - including (Li and Ding, 2026) - handle random fields by first discretizing them via Karhunen–Loève expansion (KLE), Expansion Optimal Linear Estimation (EOLE)(Li and Der Kiureghian, 1993) or spatio avearging (Geyer et al., 2022), mapping the infinite-dimensional field to a finite set of random variables before fitting a surrogate. When the spatial correlation length is small relative to the structural domain, this discretization requires a large number of terms to achieve acceptable truncation error, leading to high-dimensional inputs that strain surrogate construction.

The emergence of operator learning provides a novel paradigm for overcoming these challenges (Nikola B. Kovachki et al., 2024). By directly constructing mappings between infinite-dimensional functional spaces $\Psi : \mathcal{U} \to \mathcal{V}$, operator learning bypasses explicit KLE truncation and enables zero-shot inference on meshes of different resolutions, effectively decoupling surrogate accuracy from mesh discretization (Nelsen and Stuart, 2024; Rowbottom et al., 2026). Current approaches fall into two categories: kernel-based methods relying on Reproducing Kernel Hilbert Spaces (RKHS), such as Gaussian Process Operators (Batlle et al., 2024; Mora et al., 2025; Kumar et al., 2025), which offer mathematical interpretability, small-sample competitiveness, and built-in uncertainty quantification; and deep learning-based neural operators, including DeepONet (Lu et al., 2021), FNO (Li et al., 2021), WNO (Tripura and Chakraborty, 2023; N. et al., 2024), and PI-GLNO (Zhong and Meidani, 2024), which demonstrate strong nonlinear expressivity for parametric SPDEs. Both categories have been applied to spatiotemporal full-field reliability analysis: Gong et al. (Gong and Cheung, 2026) embedded local and global inputs into a physics-informed DeepONet with Subset Simulation, though the gradient requirement in the physical loss restricts applicability to regular grids; Tripura et al. (Tripura et al., 2024) employed a multi-fidelity wavelet neural operator validated across multiple mesh scales.

In this paper, we propose a kernel operator learning framework for spatiotemporal full-field reliability analysis under mixed random inputs, extending the RKHS-based operator learning method of Batlle et al. to the reliability setting. The framework encodes all three categories of random inputs through anisotropic product kernels on a latent GP regressor, and is paired with an active learning strategy combining integrated variance reduction near the failure region with a misclassification-based exploitation term.

The remaining sections of this paper are organized as follows: Section 2 introduces the preliminaries of spatiotemporal full-field reliability analysis and operator learning. Section 3 details the proposed physics-informed operator learning method for full-field reliability analysis. Section 4 presents a few numerical experiments to validate the effectiveness of the proposed method. Finally, Section 5 concludes the paper with a summary of findings and future research directions.

## 2. Preliminaries

### 2.1. Spatiotemporal Full-Field Reliability Analysis

Given the probability triplet $(\Omega, \mathcal{F}, \mathbb{P})$, traditional reliability analysis considers only finite-dimensional random variables $X(\omega)$ with probability measure $\mu_X$. The failure probability over domain $\Omega_{\mathcal{F}} = \{x : g(x;\omega) \leq 0\}$ is often expressed as a high-dimensional integral:

$$p_f = \mathbb{P}_\omega(\Omega_{\mathcal{F}}) = \int_{\Omega_{\mathcal{F}}} d\mu_X = \int_\Omega \mathbb{I}_{\Omega_{\mathcal{F}}}(x) p_X(x) dx \tag{1}$$

where $p_X(x)$ is the probability density function of the random variable $X(\omega)$ and $\mathbb{I}_{\Omega_{\mathcal{F}}}(x)$ is the indicator function of the failure domain.

Spatiotemporal full-field reliability analysis additionally handles stochastic processes $Y(t;\omega)$ and spatial random fields $Z(\mathbf{z};\omega)$, with probability measures $\mu_Y$ and $\mu_Z$. In the context of first passage failure, failure occurs at spatio point $z$ in a specified time interval $[0, t]$. The failure region can thus be defined as $\Omega_{\mathcal{F}} = \{(z, t, \omega) : g(z, t; \omega) \leq 0, \exists\tau \in [0, t], z \in \mathcal{D}_z\}$. Under independent assumption, the spatiotemporal failure probability is given as follows:

$$p_f(z,t) = \mathbb{P}_\omega\left(\Omega_{\mathcal{F}}\right) = \int_{\Omega_{\mathcal{F}}} d\mathbb{P}(\omega) = \int_\Omega \mathbb{I}\left(g(z,t;\omega) \leq 0\right) d\mu_X d\mu_Y d\mu_Z \tag{2}$$

### 2.2. Operator Learning

In this section, we briefly introduce some operator learning architectures. For specific operator learning theories and implementations, one can refer to (Nikola B. Kovachki et al., 2024) and (Kovachki et al., 2024). Let $\mathcal{U} = \{u : \mathcal{D}_x \to \mathbb{R}^{d_i}\}, \mathcal{D}_x \subseteq \mathbb{R}^{d_x}$ and $\mathcal{V} = \{v : \mathcal{D}_y \to \mathbb{R}^{d_o}\}, \mathcal{D}_y \subseteq \mathbb{R}^{d_y}$ be two Banach spaces. Operator learning seeks to approximate $\Psi^\dagger : \mathcal{U} \to \mathcal{V}$ with $\Psi : \mathcal{U}\times\Theta \mapsto \mathcal{V}, \Theta \subseteq \mathbb{R}^p$ from data $\{u_n, \Psi^\dagger(u_n)\}_{n=1}^N, u_n \sim \mu$, where $\mu$ is a probability measure on $\mathcal{U}$.

Since $\mathcal{U}$ and $\mathcal{V}$ are infinite-dimensional, it is necessary to project them into a finite-dimensional latent space for numerical analysis. To this end, a pair of encoder-decoder maps can be defined on $\mathcal{U}$ and $\mathcal{V}$,

$$\begin{aligned} F_{\mathcal{U}} &: \mathcal{U} \to \mathbb{R}^{d_u}, \quad G_{\mathcal{U}} : \mathbb{R}^{d_u} \to \mathcal{U} \\ F_{\mathcal{V}} &: \mathcal{V} \to \mathbb{R}^{d_v}, \quad G_{\mathcal{V}} : \mathbb{R}^{d_v} \to \mathcal{V} \end{aligned} \tag{3}$$

The encoder $F$ extracts finite-dimensional features from functional space, and the decoder $G$ maps the features back to the functional space. The latent structure mapping relationship is illustrated as shown in Figure 1. The operator can be reformulated as,

$$\Psi = G_{\mathcal{V}} \circ \varphi \circ F_{\mathcal{U}}. \tag{4}$$

$$\begin{tikzcd}
\mathcal{U} \arrow[r, "\Psi^{\dagger}"] \arrow[d, shift right, "F_{\mathcal{U}}"'] & \mathcal{V} \arrow[d, shift left, "F_{\mathcal{V}}"] \\
\mathbb{R}^{d_u} \arrow[r, "\varphi"] \arrow[u, shift right, "G_{\mathcal{U}}"'] & \mathbb{R}^{d_v} \arrow[u, shift left, "G_{\mathcal{V}}"]
\end{tikzcd}$$

*Figure 1.* Latent structure in maps between Banach spaces $\mathcal{U}$ and $\mathcal{V}$, adapted from (Nikola B. Kovachki et al., 2024)

Different encoder-decoder combinations yield different operator learning architectures. We focus below on kernel operator learning, which form the basis of the proposed framework. In DeepONet (Lu et al., 2021), $F_{\mathcal{U}}$ evaluates $u$ at fixed sensor points and $G_{\mathcal{V}}$ is a linear combination of trunk-net basis functions, giving output mesh independence but fixing the input sensor locations at inference time.

In kernel methods, $\mathcal{U}$ and $\mathcal{V}$ are assumed to be RKHSs defined by kernels $Q : \mathcal{D}_x \times \mathcal{D}_x \to \mathbb{R}$ and $K : \mathcal{D}_y \times \mathcal{D}_y \to \mathbb{R}$, which ensures the continuity of pointwise evaluations (Dirac functions). $Q$ and $K$ can be taken to be Matérn-like kernels, or any other smoother kernels such that their RKHSs are embedded in $\mathcal{U}$ and $\mathcal{V}$.

The decoders $G_{\mathcal{U}}$ and $G_{\mathcal{V}}$ are defined as the following optimal recovery maps:

$$\begin{aligned} G_{\mathcal{U}}(U) &= \operatorname*{arg\,min}_{w \in \mathcal{U}} \|w\|_Q, \quad \text{s.t. } F_{\mathcal{U}}(w) = U, \\ G_{\mathcal{V}}(V) &= \operatorname*{arg\,min}_{w \in \mathcal{V}} \|w\|_K, \quad \text{s.t. } F_{\mathcal{V}}(v) = V. \end{aligned} \tag{5}$$

where $\|\cdot\|_Q$ and $\|\cdot\|_K$ are the RKHS norms arising from their pertinent kernels. As long as the encoders $F_{\mathcal{U}}$ and $F_{\mathcal{V}}$ are linear evaluations, the optimal recovery maps Problem 5 can be solved in closed form by standard representer theorems:

$$\begin{aligned} G_{\mathcal{U}}(U)(x) &= Q(x, \mathbf{X}) Q(\mathbf{X}, \mathbf{X})^{-1} U, \\ G_{\mathcal{V}}(V)(y) &= K(y, \mathbf{Y}) K(\mathbf{Y}, \mathbf{Y})^{-1} V. \end{aligned} \tag{6}$$

where $Q(\mathbf{X}, \mathbf{X})$ and $K(\mathbf{Y}, \mathbf{Y})$ are the kernel matrices with entries $Q(\mathbf{X}, \mathbf{X})_{ij} = Q(\mathbf{X}_i, \mathbf{X}_j)$ and $K(\mathbf{Y}, \mathbf{Y})_{ij} = K(\mathbf{Y}_i, \mathbf{Y}_j)$ respectively. The latent mapping $\varphi$ is approximated by ridge regression:

$$\varphi = \operatorname*{arg\,min}_{w} \|w\|_{\Gamma}, \text{ s.t. } w(F_{\mathcal{U}}(u_n)) = F_{\mathcal{V}}(v_n), n = 1, \ldots, N \tag{7}$$

where $\|\cdot\|_{\Gamma}$ is the RKHS norm of the matrix kernel $\Gamma$ defined on the latent space. When performing mesh independent inference, two additional encoders $\tilde{F}_{\mathcal{U}}$ and $\tilde{F}_{\mathcal{V}}$ and decoders $\tilde{G}_{\mathcal{U}}$ and $\tilde{G}_{\mathcal{V}}$ can be introduced to map between RKHSs and finite-dimensional latent spaces, and the corresponding learned operator can be expressed as:

$$\Psi = \tilde{F}_{\mathcal{V}} \circ G_{\mathcal{V}} \circ \varphi \circ F_{\mathcal{U}} \circ \tilde{G}_{\mathcal{U}} \tag{8}$$

## 3. Methodology

In this section, we present an adaptive kernel operator learning framework for spatiotemporal full-field reliability analysis under mixed random inputs.

### 3.1. Improved Kernel Operator Learning for Spatiotemporal Full-Field Reliability Analysis

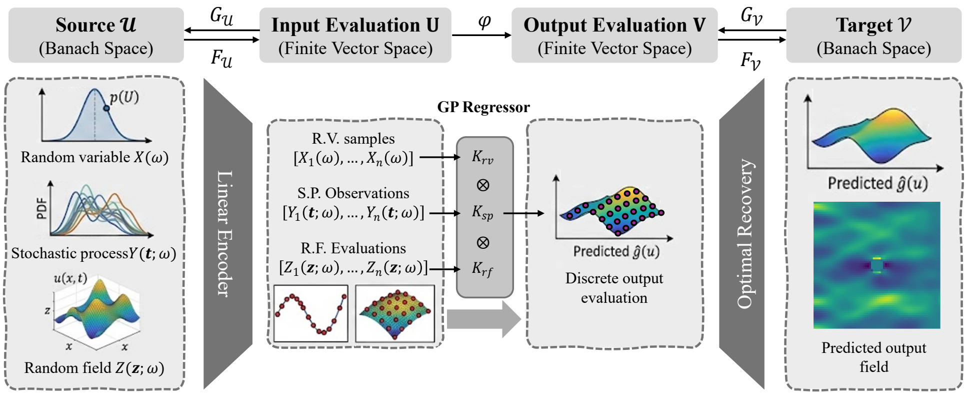


*Figure 2.* The architecture of the proposed kernel operator learning framework for spatiotemporal full-field reliability analysis.

As reviewed in Section 2.2, kernel operator learning involves three key components: the input function encoder $F_{\mathcal{U}}$, the output function decoder $G_{\mathcal{V}}$, and the latent mapping $\varphi$. The overall architecture of the proposed kernel operator learning framework is illustrated in Figure 2. The following sections detail the specific design choices for each component, with a focus on how they are tailored to the spatiotemporal full-field reliability analysis setting.

#### 3.1.1. *Choice of Encoder and Decoder*

Following (Batlle et al., 2024), we adopt linear encoders and decoders constructed from the Cholesky factors of the input and output kernel matrices,

$$Q(\mathbf{X},\mathbf{X})^{-1} = L_Q L_Q^T, \quad K(\mathbf{Y},\mathbf{Y})^{-1} = L_K L_K^T. \tag{9}$$

The input RKHS uses a Matérn-1/2 kernel to accommodate the non-smooth sample paths of stochastic processes and random fields, while the output RKHS uses a Gaussian kernel, reflecting the smoothing effect of the underlying PDE operator.

### 3.1.2. *Latent mapping*

The core of the operator learning framework lies in approximating the mapping between the projected finite-dimensional latent coordinates. In this study, an operator-valued Gaussian Process (GP) is utilized as the surrogate model for this latent mapping, since it provides a non-parametric, flexible representation of the mapping with built-in uncertainty quantification.

In common settings, the matrix valued kernel $\Gamma : \mathbb{R}^{d_u} \times \mathbb{R}^{d_u} \to \mathbb{R}^{d_v}$ is utilized to define the covariance structure of the operator-valued GP. To maintain a balance between model expressivity and computational tractability, a simple and practical choice for $\Gamma$ is the diagonal kernel

$$\Gamma(\mathbf{U}, \mathbf{U}') = K(\mathbf{U}, \mathbf{U}') \cdot \mathbf{I}, \tag{10}$$

where $K : \mathbb{R}^{d_u} \times \mathbb{R}^{d_u} \to \mathbb{R}$ is an arbitary scalar valued kernel, such as Gaussian, Matérn, or rational quadratic kernels.

In spatiotemporal full-field reliability analysis, the uncertain inputs comprise three structurally distinct categories: finite-dimensional random variables $X(\omega) \in \mathbb{R}^{d_X}$, stochastic processes $Y(t;\omega)$ indexed over time $t \in \mathcal{T}$, and spatial random fields $Z(\mathbf{z};\omega)$ indexed over the spatial domain $\mathcal{D}$. To capture the distinct physical influences and correlation structures of different uncertainty sources, we construct anisotropic kernels within this GP framework. Therefor, we define the extended input space as the product space

$$\mathcal{U} = \mathbb{R}^{d_X} \oplus \mathcal{U}_Y \oplus \mathcal{U}_Z, \tag{11}$$

where $\mathcal{U}_Y$ is the RKHS of stochastic processes over $\mathcal{T}$, and $\mathcal{U}_Z$ is the RKHS of spatial random fields over $\mathcal{D}$. A realization of the joint input is denoted $u = (x, y(\cdot), z(\cdot)) \in \mathcal{U}$.

Three anisotropic kernels are defined for each input type. For random variables, stochastic processes, and spatial random fields, we respectively adopt:

$$\begin{aligned} K_{\mathrm{rv}}(X, X') &= \exp\!\left(-\tfrac{1}{2}(X - X')^T \Lambda^{-2} (X - X')\right), \\ K_{\mathrm{sp}}(Y, Y') &= k^{\nu}_{\mathrm{Matérn}}\!\left(\|\mathbf{t} - \mathbf{t}'\|;\, \ell_t\right), \\ K_{\mathrm{rf}}(Z, Z') &= \sigma_Z^2\, k^{\nu}_{\mathrm{Matérn}}(r; \ell), \quad r = \left\|\Lambda_Z^{-1}(\mathbf{Z} - \mathbf{Z}')\right\|, \end{aligned} \tag{12}$$

where $\Lambda = \mathrm{diag}(\ell_1, \ldots, \ell_{d_X})$ and $\Lambda_Z$ encode per-dimension length-scales for random variables and spatial random fields respectively. Unlike KLE or EOLE, $d_z$ affects only the Gram matrix size in the optimal recovery map, not the dimensionality of the regression problem.

The three kernels are combined via a tensor product to form the joint input kernel:

$$\Gamma\big((X, Y, Z), (X', Y', Z')\big) = K_{\mathrm{rv}}(X, X') \otimes K_{\mathrm{sp}}(Y, Y') \otimes K_{\mathrm{rf}}(Z, Z'). \tag{13}$$

The posterior mean and covariance of the operator-valued GP with kernel $\Gamma$ can be expressed as

$$\begin{aligned} \hat{v}_* &= \mu(\mathbf{x}_*) + \Gamma(\mathbf{x}_*, \mathbf{X})[\Gamma(\mathbf{X}, \mathbf{X}) + \sigma_n^2 \mathbf{I}]^{-1}(\mathbf{y} - \mu(\mathbf{X})) \\ \hat{\sigma}^2 &= \Gamma(\mathbf{x}_*, \mathbf{x}_*) - \Gamma(\mathbf{x}_*, \mathbf{X})[\Gamma(\mathbf{X}, \mathbf{X}) + \sigma_n^2 \mathbf{I}]^{-1}\Gamma(\mathbf{x}_*, \mathbf{X}) \end{aligned} \tag{14}$$

### 3.2. Active Learning Strategy for Kernel Operator Learning

The kernel operator learning surrogate $\Psi$ is trained on a dataset $\{u_n, \Psi^\dagger(u_n)\}_{n=1}^N$, where each pair requires one evaluation of the underlying PDE solver. Since such evaluations are computationally expensive, it is desirable to select training samples adaptively to characterize the spatiotemporal limit state boundary with as few solver calls as possible. Active learning for reliability analysis has been well-established in the Kriging setting (Echard et al., 2011; Moustapha, 2016), with strategies developed for time-invariant, time-variant, and multi-fidelity problems (Song et al., 2026; Zhao et al., 2026; Feng et al., 2025). The present operator learning setting differs in two key respects: the input is a function-valued source $u \in \mathcal{U}$, and the surrogate output is a full spatiotemporal field $v \in \mathcal{V}$, so model uncertainty is a global quantity and the limit state boundary is a zero level set in $\mathcal{U}$ rather than a hypersurface in $\mathbb{R}^d$.

#### 3.2.1. *Learning Function*

According to Eqs 14, the learned kernel operator model provides, for any candidate input $U^* = F_{\mathcal{U}}(u^*)$, a posterior mean $\hat{v}_k(U^*)$ and variance $\sigma_k^2(U^*)$ at each output observation point $y_k \in Y$, $k = 1, \ldots, d_V$. The active learning strategy seeks the next most informative sample over a candidate pool $\mathcal{C} = \{U_j\}_{j=1}^M$, balancing global exploration with local exploitation near the limit state boundary. We construct the acquisition function as a weighted combination of two terms.

The global term quantifies the expected reduction in predictive uncertainty over the current candidate pool $\mathcal{C} = \{U_j\}_{j=1}^M$ if $U^*$ is added to the DoE. For a GP with posterior variance $\sigma_t^2(U)$ at iteration $t$, the one-step variance reduction at an arbitrary point $U \in \mathcal{U}$ after observing $U^*$ follows directly from the GP update equations:

$$\sigma_t^2(U) - \sigma_{t+1,U^*}^2(U) = \frac{\Gamma(U, U^*)^2}{\Gamma(U^*, U^*) + \gamma}, \tag{15}$$

where $\Gamma(\cdot, \cdot)$ is the posterior covariance of the latent mapping $\varphi$ and $\gamma > 0$ is a noise regularization constant. Integrating this reduction over the input measure $\mu$ and approximating the integral by a Monte Carlo Simulation (MCS) over the candidate pool gives the standard IVR acquisition function:

$$\alpha_{\mathrm{IVR}}(U^*) = \int_{\mathcal{U}} \big[\sigma_t^2(U) - \sigma_{t+1,U^*}^2(U)\big] \mathrm{d}\mu(U) \approx \frac{1}{M(\sigma_{\mathrm{signal}}^2 + \gamma)} \sum_{j=1}^{M} \Gamma(U_j, U^*)^2, \tag{16}$$

where $\sigma_{\mathrm{signal}}^2 \approx \Gamma(U^*, U^*)$ is the prior signal variance. To concentrate exploration near the limit state boundary, we reweight each candidate by:

$$w_j = \frac{\Phi\big(|\hat{v}_{\min}(U_j)|/\sigma_{\min}(U_j)\big)}{\sum_{j'} \Phi\big(|\hat{v}_{\min}(U_{j'})|/\sigma_{\min}(U_{j'})\big)}, \tag{17}$$

where $\hat{v}_{\min}(U_j) = \min_k \hat{v}_k(U_j)$ is the predicted minimum response over the spatiotemporal domain and $\Phi$ is the standard normal PDF. The corresponding weighted integrated variance reduction acquisition function is

$$\alpha_{\text{IVR-zero}}(U^*) \approx \frac{1}{M(\sigma_{\mathrm{signal}}^2 + \gamma)} \sum_{j=1}^{M} w_j \cdot \Gamma(U_j, U^*)^2. \tag{18}$$

The local exploitation term sums the sign-misclassification probability over all output points:

$$\alpha_{\mathrm{MIS}}(U^*) = \sum_{k=1}^{d_V} \Phi\left(-\frac{|\hat{v}_k(U^*)|}{\sigma_k(U^*)}\right). \tag{19}$$

The two terms are then combined with an adaptive weight $\lambda_t = \lambda_0(1 - e^{-t/\tau})$ that balances global exploration early in the learning process against local exploitation as the level set estimate matures:

$$U^* = \arg\max_{U \in \mathcal{C}} \alpha(U) = \arg\max_{U \in \mathcal{C}} \alpha_{\text{IVR-zero}}(U) + \lambda_t \, \alpha_{\mathrm{MIS}}(U) \tag{20}$$

#### 3.2.2. *Stopping Criterion*

Aside from the learning function, another essential aspect of active learning is the stopping criterion. In this study, we propose a criterion based on the stability of the estimated spatiotemporal limit state boundary.

We track the discrete zero level set of the surrogate over the candidate pool:

$$\hat{\mathcal{L}}_t = \left\{ j \in \mathcal{I}_{\text{avail}} : \hat{v}_{\min}^{(j)} < 2 \right\}, \tag{21}$$

where $\mathcal{I}_{\text{avail}}$ indexes the available candidate samples and the threshold 2 provides a margin around the zero level set. The relative change rate of the level set at iteration $t$ and its moving average are defined as

$$\Delta_t = \frac{\big||\hat{\mathcal{L}}_t| - |\hat{\mathcal{L}}_{t-1}|\big|}{|\hat{\mathcal{L}}_t| + \epsilon}, \quad \bar{\Delta}_t = \frac{1}{K} \sum_{k=1}^{K-1} \Delta_{t-k}. \tag{22}$$

where $\epsilon > 0$ is a small constant preventing division by zero. The active learning loop terminates when $\bar{\Delta}_t < \tau_\Delta$, where $\tau_\Delta$ is a user-specified tolerance. This criterion directly measures the stability of the reliability-relevant region of the input space rather than the overall surrogate accuracy, making it well-suited for reliability analysis where only the sign of the limit state function matters. In ouir practice, the tolerance $\tau_\Delta$ can be around 0.001 to 0.005, and the moving average window size $K$ can be around 20, depending on the problem complexity and computational budget.

### 3.3. Implementation Procedure of Proposed Method

The overall procedure is summarized in Figure 3.

## 4. Numerical Experiments

In this section, we present three numerical examples using either numerical solvers or finite element solvers to demonstrate the effectiveness of the proposed method.

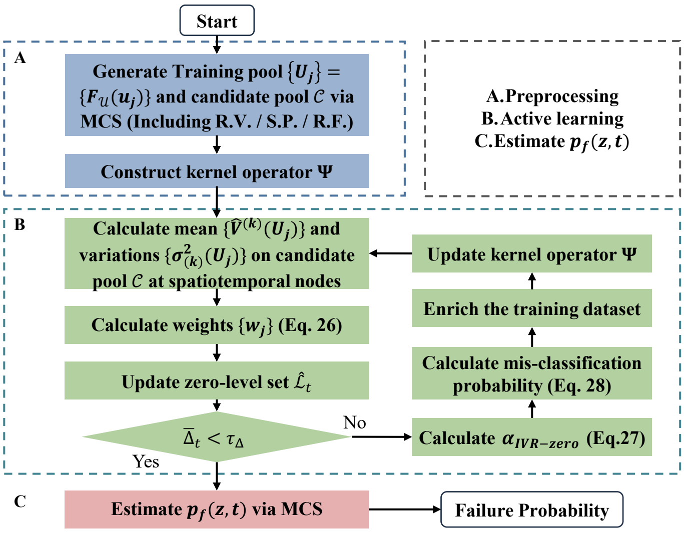


*Figure 3.* Flowchart of the proposed active learning strategy

### 4.1. Example 1: 1D Poisson Equation

We first consider a parametric 1D Poisson equation with a stochastic forcing term:

$$-\alpha(\omega)\frac{d^2u(x;\omega)}{dx^2} = f(x;\omega), \quad x \in [0,1], \quad u(0;\omega) = u(1;\omega) = 0. \tag{23}$$

where the uncertain parameter $\alpha = \beta^2 + 1, \beta \sim \mathcal{N}(0,1)$; the stochastic forcing $f(t;\omega)$ will be considered as stationary Gaussian process,

$$f(x;\omega) \sim \mathcal{GP}\left(0, \exp\left(-\frac{(x-x')^2}{2l^2}\right)\right), l = 0.3. \tag{24}$$

We first analyze the performance of kernel operator learning without active learning, where the training dataset consists of $N = 300$ samples of $\alpha$ and $f$ generated by Monte Carlo sampling. The input RKHS is equipped with a Matérn 1/2 kernel with the same correlation length of $l = 0.3$, while the output RKHS is equipped with a RBF kernel with correlation length of $l = 0.5$. The forcing term $f(x;\omega)$ and corresponding output displacement $u(x)$ is evaluated on a 51-point uniform grid, and two test datasets are generated on the same grid and a finer 101-point grid with $10^4$ samples each, in order to demonstrate the ability for operator learning to generalize to different output meshes. Five representative test samples are visualized in Figure 4a and Figure 4b. The relative $L^2$ error on two test datasets are 2.83% and 2.91% respectively.

The limit state function of each spatial point is defined as $g(x) = |0.75 - u(x)|$. Given the trained kernel operator, the failure probability is estimated by performing a Monte Carlo Simulation over two test datasets inputs, as shown in Figure 4c. The surrogate failure probability estimates agree well with the reference, as shown in Figure 4.

We then turn to adaptive sampling with the proposed active learning strategy, where the initial training dataset consists of $N_0 = 20$ samples and the candidate pool consists of $N_{\text{MCS}} = 10^4$

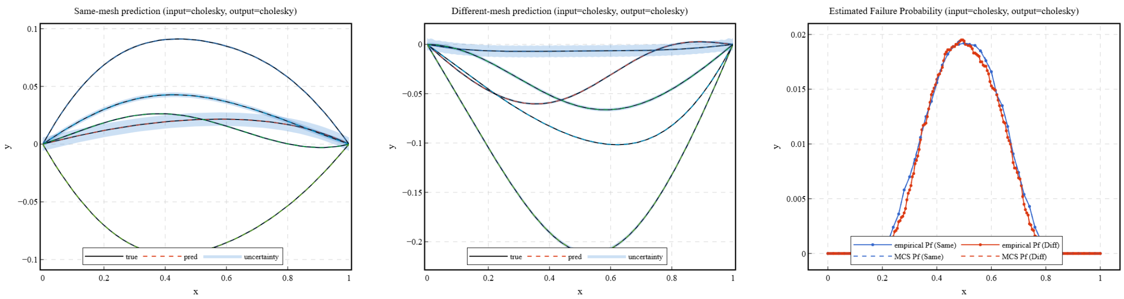


(a) Same grid prediction of $u(x;\omega)$

(b) Finer grid prediction of $u(x;\omega)$

(c) Failure probability estimation

*Figure 4.* 1D Poisson equation Results

samples. Parameter $\tau_\Delta$ and $K$ are set to 0.005 and 20 respectively. Figure 5a and Figure 5b shows the convergence of the active learning strategy. After 93 iterations, the adaptive strategy converges and the final surrogate is used to estimate the failure probability, result of which is given in Figure 5c. Compared to the result without adaptive sampling strategy, it reaches a similar accuracy with only 93 training samples, which demonstrates the efficiency of the proposed active learning strategy in identifying informative training samples and accelerating the learning process.

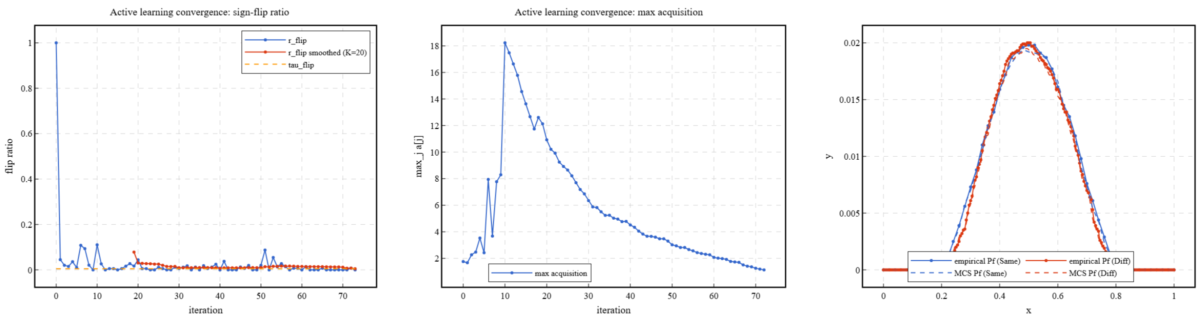


(a) Stability of zero level set

(b) Learning function value

(c) Failure probability estimation

*Figure 5.* Results of the active learning strategy for the 1D Poisson equation

## 4.2. Example 2: Diffusion Reaction PDE

We next consider a 2D diffusion-reaction PDE with a stochastic source term:

$$\frac{\partial u(x,t;\omega)}{\partial t} = \frac{\partial}{\partial x}\left(K(x;\omega)\frac{\partial u(x,t;\omega)}{\partial x}\right) + 0.01\,u(x,t;\omega)^2 + f(x;\omega), \quad (x,t) \in [0,1]\times[0,1] \quad (25)$$

where the diffusion term is defined a $K(x;\omega) = 0.01(\sin(k(x;\omega)) + 2)$. Two independent input random fields are given as:

$$k(x;\omega) \sim \mathcal{GP}\left(2,\ 0.25^2 \exp\left(-\frac{(x-x')^2}{2l^2}\right)\right), f(x;\omega) \sim \mathcal{GP}\left(5,\ \exp\left(-\frac{(x-x')^2}{2l^2}\right)\right), l = 0.3. \tag{26}$$

The training dataset consists of $N = 200$ samples of $k$ and $f$ generated by Cholesky decomposition. The RKHS kernels are chosen as Matérn 1/2 and RBF kernels with correlation lengths of $l = 0.3$ and $l = 0.5$, respectively. $f(x;\omega)$, $k(x;\omega)$ and corresponding output displacement $u(x,t)$ is evaluated on a uniform grid with $n_x \times n_t = (41 \times 21)$, and two test datasets are generated on the same grid and a finer $(101 \times 81)$ grid with $10^4$ samples each. A representative test samples are visualized in Figure 6a, Figure 6b and Figure 6c. The relative $L^2$ error on two test datasets are 0.08% and 0.70% respectively. The lower error relative to Example 1 is attributable to the smoothing effect of diffusion.

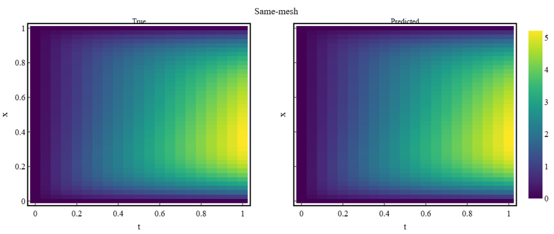


(a) Same grid prediction of $u(x,t;\omega)$

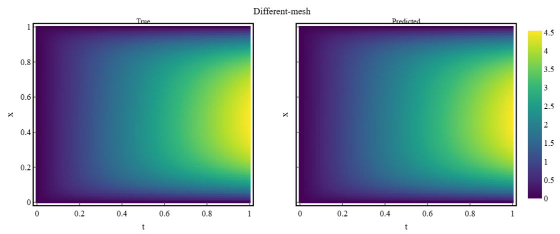


(b) Finer grid prediction of $u(x,t;\omega)$

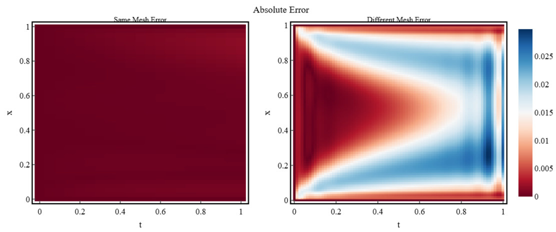


(c) Absolute error of $u(x,t;\omega)$

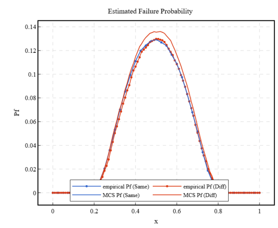


(d) Failure probability estimation

*Figure 6.* Predictions of the kernel operator learning surrogate for the diffusion-reaction PDE

Since it is a time variant problem, the limit state function of each spatial point is defined as a first passage problem $g(x,t) = 6 - \max_t u(x,t;\omega)$. Given the trained kernel operator, the first passage failure probability is estimated by Monte Carlo Simulation over two test datasets inputs. The results are given in Figure 6d, where same mesh prediction outperforms finer mesh prediction as operator learning indeed in theory is a data-driven method and thus gives less accurate predictions on unseen meshes.

Considering adaptive sampling strategy, the initial training dataset consists of $N_0 = 20$ samples and the candidate pool consists of $N_{\text{MCS}} = 10^4$ samples. Parameter $\tau_\Delta$ and $K$ are set to 0.001 and 20 respectively. Figure 7a and Figure 7b shows the convergence of the active learning strategy, where we can see that after 82 iterations, the active learning strategy converges and the final surrogate is used to estimate the failure probability, result of which is given in Figure 7c. Compared to the result without adaptive sampling strategy, it reaches a similar accuracy with only 42 training samples, which demonstrates the efficiency of the proposed active learning strategy in identifying informative training samples and accelerating the learning process.


(a) Stability of zero level set (b) Learning function value (c) Failure probability estimation

*Figure 7.* Results of the active learning strategy for the diffusion reaction problem

### 4.3. Example 3: Planar Stress of Plates with a Hole

In this example, we consider a 2D planar stress problem of a plate with a hole under tension, where the Young's modulus is modeled as a spatial random field. The problem is posed on the perforated domain $\Omega = [0,2]^2 \setminus \{(x,y) : (x-1)^2 + (y-1)^2 \leq 0.1^2\}$, with equilibrium equation and boundary conditions:

$$\begin{cases} \nabla \cdot \boldsymbol{\sigma} = \mathbf{0}, & \forall (x,y) \in \Omega, \\ u(x,y) = 0, & x = 0, \\ \boldsymbol{\sigma} \cdot \mathbf{n} = p_0 \mathbf{e}_x, & x = 2. \end{cases} \tag{27}$$

where $\boldsymbol{\sigma}$ is the stress tensor, $\mathbf{n}$ is the outward normal vector, and $p_0$ is the applied tension on the boundary. Kernel operator learning aims to learn the mapping from Young's modulus to the von-mises stress field. The Young's modulus $E(x, y; \omega)$ is modeled as a log-normal random field:

$$Z(x,y) = \ln\left(\frac{E(x,y)}{E_0}\right), \quad \mathrm{Cov}[Z(\mathbf{s}), Z(\mathbf{s}')] = \sigma_Z^2 \frac{r}{\ell} K_1\left(\frac{r}{\ell}\right), \quad r = \|\mathbf{s} - \mathbf{s}'\| \tag{28}$$

As kernel operators are both input and output mesh independent, we consider two training cases in this example. In both cases, the input is evaluated via SPDE method (Lindgren et al., 2011) and the problem is solved by finite element method. The training dataset contains $N = 1000$ samples, while two other test datasets contain $10^4$ samples each. The limit state function is given as $g(x, y) = 3p_0 - \sigma(x, y)$.

#### 4.3.1. *Case 1*

In the first case, we use uniform mesh of $51 \times 51$ elements as training grid and both $51 \times 51$ uniform and unstructured meshes of 4720 elements as test grids. Results of one of the prediction is shown in Figure 8, where we can see that both test meshes give acceptable predictions, with relative $L^2$

errors of 7.25% and 9.13%. The results of further failure probability estimation is demonstrated in Figure 9. The unstructured-mesh estimates are less accurate, as the coarser training mesh (2061 elements) contains less information than the 4720-element test mesh.

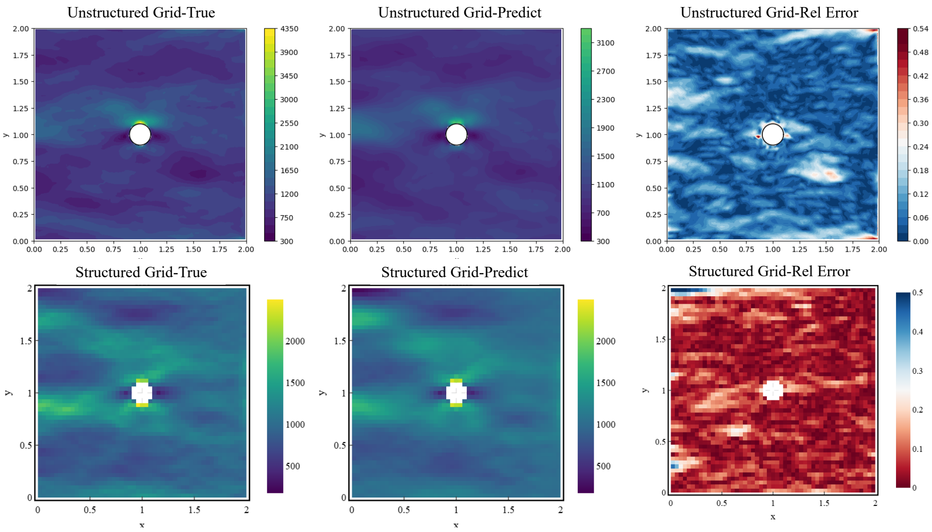


*Figure 8.* Predictions of the kernel operator for planar stress problem

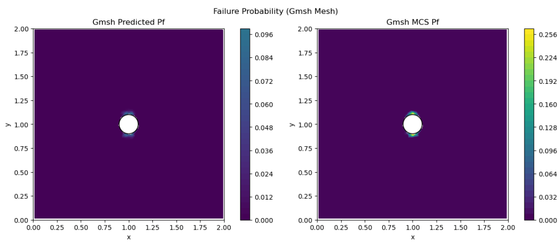


(a) Failure probability estimation on unstructured mesh

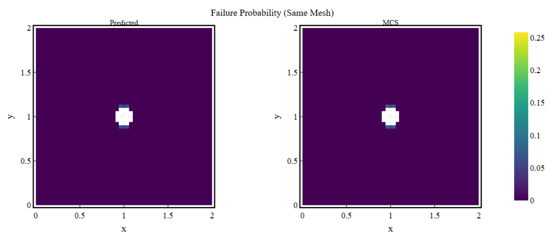


(b) Failure probability estimation on uniform mesh

*Figure 9.* Failure probability estimation for planar stress case 1

### 4.3.2. *Case 2*

In the second case, we use unstructured mesh of 4720 elements as training grid and both uniform of $51 \times 51$ elements and unstructured meshes as test grids. One of the prediction is given in Figure 10, where we can see that both test meshes give acceptable predictions, with relative $L^2$ errors of 8.97% and 7.94%. The results of further failure probability estimation is demonstrated in Figure 11. Consistent with Case 1, training on the finer mesh reduces both prediction and failure probability estimation error.

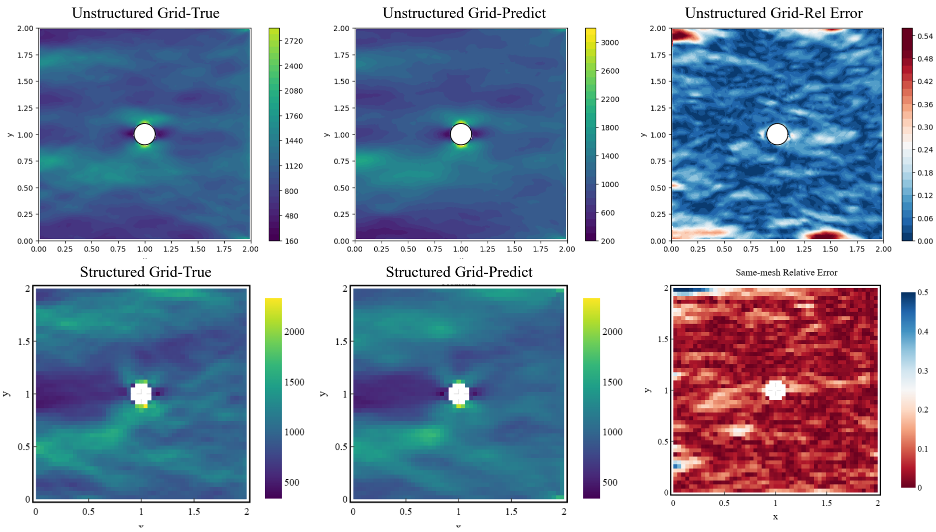


*Figure 10.* Predictions of the kernel operator for planar stress problem

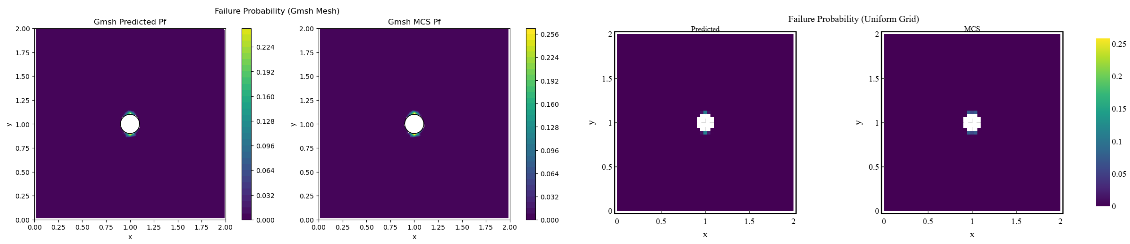


(a) Failure probability estimation on unstructured mesh

(b) Failure probability estimation on uniform mesh

*Figure 11.* Failure probability estimation for planar stress case 2

## 5. Conclusion

This paper presented a kernel operator learning framework for spatiotemporal full-field reliability analysis under mixed random inputs. By extending the RKHS-based operator learning method of Batlle et al. to the reliability setting, the proposed framework constructs a surrogate that directly maps random variables, stochastic processes, and spatial random fields to the full spatiotemporal response field, without prior discretization via KLE or EOLE. The three input types are encoded through anisotropic product kernels on the latent GP regressor, each tailored to its corresponding covariance structure. An active learning strategy was further developed, combining an IVR-based global exploration term weighted toward the zero level set with a local sign-misclassification exploitation term, and terminated by a level-set stability criterion. The framework was validated on two benchmark problems: a 1D spatial Poisson equation with mixed random variable and random field inputs, and a 2D spatiotemporal diffusion-reaction equation with random process and random field inputs.

Two directions are identified for future work. First, the present learning function targets uncertainty reduction near the zero level set, but its quantitative contribution to failure probability accuracy is not explicitly tracked. A more principled formulation would optimize directly for the expected reduction in the variance of $\hat{p}_f$, analogous to (Song, 2022), extended to the operator setting where the failure event is defined by a spatiotemporal supremum. Second, the Cameron–Martin theorem establishes that random field sample paths belong to the associated RKHS only on a set of measure zero, creating a mismatch between the assumed function space geometry and the actual field distribution. Kernel Flows (Owhadi and Yoo, 2019) offers a data-driven remedy by adaptively learning kernel parameters to align the RKHS geometry with observed field realizations, replacing the current manual specification of Matérn smoothness and length-scale parameters.

## References


Batlle, P., M. Darcy, B. Hosseini, and H. Owhadi: 2024, 'Kernel Methods Are Competitive for Operator Learning'. *Journal of Computational Physics* **496**, 112549.

Cao, R., Z. Sun, J. Wang, and F. Guo: 2022, 'A Single-Loop Reliability Analysis Strategy for Time-Dependent Problems with Small Failure Probability'. *Reliability Engineering & System Safety* **219**, 108230.

Dimitrov, N., R. D. Bitsche, and J. P. Blasques: 2017, 'Spatial Reliability Analysis of a Wind Turbine Blade Cross Section Subjected to Multi-Axial Extreme Loading'. *Structural Safety* **66**, 27–37.

Echard, B., N. Gayton, and M. Lemaire: 2011, 'AK-MCS: An Active Learning Reliability Method Combining Kriging and Monte Carlo Simulation'. *Structural Safety* **33**(2), 145–154.

Feng, S., L. Wang, H. Dong, Y. Li, Z. Wan, and C. G. Soares: 2025, 'An Active-Learning Method Based on Hierarchical Kriging Model for Multi-Fidelity Reliability Analysis'. *Reliability Engineering & System Safety* p. 111759.

Geyer, S., I. Papaioannou, L. Graham-Brady, and D. Straub: 2022, 'The Spatial Averaging Method for Non-Homogeneous Random Fields with Application to Reliability Analysis'. *Engineering Structures* **253**, 113761.

Gong, Y. and S. H. Cheung: 2026, 'Adaptive Physics-Informed Neural Operator and Subset Simulation for High-Dimensional Reliability Analysis with Multiple Stochastic Processes in Stochastic Differential Equations'. *Reliability Engineering & System Safety* **268**, 111949.

Hu, W., J. Liao, J. Yan, J. Fang, F. Zhao, I. Lee, and J. Tan: 2026, 'Spatiotemporal-Dependent Reliability Analysis with Adaptive Sampling Physics-Informed Neural Networks'. *Reliability Engineering & System Safety* **265**, 111560.

Kovachki, N., Z. Li, B. Liu, K. Azizzadenesheli, K. Bhattacharya, A. Stuart, and A. Anandkumar: 2024, 'Neural Operator: Learning Maps between Function Spaces'.

Kumar, S., R. Nayek, and S. Chakraborty: 2025, 'Towards Gaussian Process for Operator Learning: An Uncertainty Aware Resolution Independent Operator Learning Algorithm for Computational Mechanics'. *Computer Methods in Applied Mechanics and Engineering* **435**, 117664.

Li, C.-C. and A. Der Kiureghian: 1993, 'Optimal Discretization of Random Fields'. *Journal of Engineering Mechanics* **119**(6), 1136–1154.

Li, X. and C. Ding: 2026, 'Active Evolutionary Gaussian Process for Structural Large-Scale Full-Field Reliability Analysis and Critical Domain Prognosis with Only Few Initial Samples'. *Computer Methods in Applied Mechanics and Engineering* **448**, 118418.

Li, X.-W., Y.-G. Zhao, X.-Y. Zhang, and Z.-H. Lu: 2022, 'Explicit Model of Outcrossing Rate for Time-Variant Reliability'. *ASCE-ASME Journal of Risk and Uncertainty in Engineering Systems, Part A: Civil Engineering* **8**(1), 4021087.

Li, Z., N. Kovachki, K. Azizzadenesheli, B. Liu, K. Bhattacharya, A. Stuart, and A. Anandkumar: 2021, 'Fourier Neural Operator for Parametric Partial Differential Equations'.

Lindgren, F., H. Rue, and J. Lindström: 2011, 'An Explicit Link between Gaussian Fields and Gaussian Markov Random Fields: The Stochastic Partial Differential Equation Approach'. *Journal of the Royal Statistical Society Series B: Statistical Methodology* **73**(4), 423–498.

Lu, L., P. Jin, G. Pang, Z. Zhang, and G. E. Karniadakis: 2021, 'Learning Nonlinear Operators via DeepONet Based on the Universal Approximation Theorem of Operators'. *Nature Machine Intelligence* **3**(3), 218–229.

Lu, Z.-H., H.-P. Qiao, X.-Y. Zhang, and Y.-G. Zhao: 2023, 'An Innovative Method for Space-Time-Dependent Reliability Analysis'. *Structural Safety* **102**, 102326.

Mora, C., A. Yousefpour, S. Hosseinmardi, H. Owhadi, and R. Bostanabad: 2025, 'Operator learning with gaussian processes'. *Computer Methods in Applied Mechanics and Engineering* **434**, 117581.

Moustapha, M.: 2016, 'Adaptive Surrogate Models for the Reliable Lightweight Design of Automotive Body Structures'. Ph.D. thesis, BLAISE PASCAL UNIVERSITY – CLERMONT II.

N., N., T. Tripura, and S. Chakraborty: 2024, 'Physics Informed WNO'. *Computer Methods in Applied Mechanics and Engineering* **418**, 116546.

Nelsen, N. H. and A. M. Stuart: 2024, 'Operator Learning Using Random Features: A Tool for Scientific Computing'. *SIAM Review* **66**(3), 535–571.

Nikola B. Kovachki, Samuel Lanthaler, and Andrew M. Stuart: 2024, 'Chapter 9 - Operator Learning: Algorithms and Analysis'. In: *Numerical Analysis Meets Machine Learning*, Vol. 25 of *Handbook of Numerical Analysis*. Elsevier, pp. 419–467.

Owhadi, H. and G. R. Yoo: 2019, 'Kernel Flows: From Learning Kernels from Data into the Abyss'. *Journal of Computational Physics* **389**, 22–47.

Rowbottom, J., S. Fresca, P. Lio, C.-B. Schönlieb, and N. Boullé: 2026, 'Multi-Level Monte Carlo Training of Neural Operators'. *Computer Methods in Applied Mechanics and Engineering* **453**, 118800.

Roy, A., T. Chatterjee, and S. Adhikari: 2024, 'A Physics-Informed Neural Network Enhanced Importance Sampling (PINN-IS) for Data-Free Reliability Analysis'. *Probabilistic Engineering Mechanics* **78**, 103701.

Song, Z.: 2022, 'An Estimation Variance Reduction-Guided Adaptive Kriging Method for Efficient Time-Variant Structural Reliability Analysis'. *Mechanical Systems and Signal Processing*.

Song, Z., C. Dang, M. A. Valdebenito, and M. G. R. Faes: 2026, 'Active Learning Kriging with Functional Dimension Reduction for Reliability Analysis of Stochastic Dynamical Systems'. *Reliability Engineering & System Safety* **273**, 112360.

Tripura, T. and S. Chakraborty: 2023, 'Wavelet Neural Operator for Solving Parametric Partial Differential Equations in Computational Mechanics Problems'. *Computer Methods in Applied Mechanics and Engineering* **404**, 115783.

Tripura, T., A. Thakur, and S. Chakraborty: 2024, 'Multi-fidelity wavelet neural operator surrogate model for time-independent and time-dependent reliability analysis'. *Probabilistic Engineering Mechanics* **77**, 103672.

Zhan, H., H. Liu, and N.-C. Xiao: 2026, 'An active learning multi-fidelity kriging model for predicting the expected lifetime of time- and space-dependent structural systems with multi-fidelity data'. *Reliability Engineering & System Safety* **270**, 112192.

Zhan, H. and N.-C. Xiao: 2025, 'A New Active Learning Surrogate Model for Time- and Space-Dependent System Reliability Analysis'. *Reliability Engineering & System Safety* **253**, 110536.

Zhang, C. and A. Shafieezadeh: 2022, 'Simulation-Free Reliability Analysis with Active Learning and Physics-Informed Neural Network'. *Reliability Engineering & System Safety* **226**, 108716.

Zhao, Q., X. Jia, B. Li, M. Wang, G. Jin, and B. Guo: 2026, 'AK-TSYS: An Enhanced Active Learning Kriging Model for Time-Dependent System Reliability Analysis'. *Reliability Engineering & System Safety* **268**, 111991.

Zhao, Y., J. Liu, and Y. Ren: 2025, 'Rapid Uncertainty Quantification for Structural Full-Field Dynamic Responses with Extremely High Dimension'. *Reliability Engineering & System Safety* **261**, 111097.

Zhong, W. and H. Meidani: 2024, 'Physics-Informed Geometry-Aware Neural Operator'.